

Recovery of depth information from optical microscope images by constrained deconvolution

C.A. Glasbey

Biomathematics and Statistics Scotland
JCMB, King's Buildings, Edinburgh EH9 3JZ, Scotland, UK

M.G. Perkins

Edinburgh Parallel Computing Centre, University of Edinburgh,
JCMB, King's Buildings, Edinburgh EH9 3JZ, Scotland, UK

Abstract

A rigorous, new, depth-from-focus algorithm is proposed: microscope images at a series of focal planes are jointly deconvolved, subject to the constraint that the recovered specimen is a two-dimensional surface. A quadratic program is used to estimate the point-spread function of the optical system. Then, depth and brightness are estimated at each location on the surface by minimising a sum of squares plus roughness penalty, using a simulated annealing schedule. The algorithm has been implemented in parallel on a Cray-T3D, and the method is illustrated using brightfield optical sections of a diatom.

1 Introduction

Optical microscopes are much cheaper than electron and confocal microscopes. Although they produce images of poorer quality, digital methods can be used to enhance them. Fig 1 shows a series of brightfield optical microscope images of a diatom, a single-celled alga, at four focal planes. This is an example of optical sectioning, in which a series of images are taken of a specimen with the optical system focused at different depths perpendicular to the focal plane of the microscope. Different parts of the specimen are in focus in each image, but these can be obscured or made ambiguous by unfocused information from other parts of the specimen. In Fig 1, focal plane $k = 5$ is above the top surface of the diatom, resulting in a slightly blurred appearance, although the centre of the diatom is less blurred than the rest. At the slightly lower focal plane, $k = 7$, most of the diatom is in focus. However, the edges of the diatom are most in focus when $k = 9$ and 11, which are still lower focal planes.

Digital methods can facilitate the extraction of information from microscope images such as Fig 1. Two areas where there has been considerable activity are *deconvolution*, which improves the resolving power of microscopes, and *depth-from-focus*, where three-dimensional information is inferred from the extent of blur in images. For incoherent light, blur is a linear convolution of the optical density of a microscope specimen [6]. Therefore, the pixel value at location (i, j) in the digital image at focal plane k is specified by

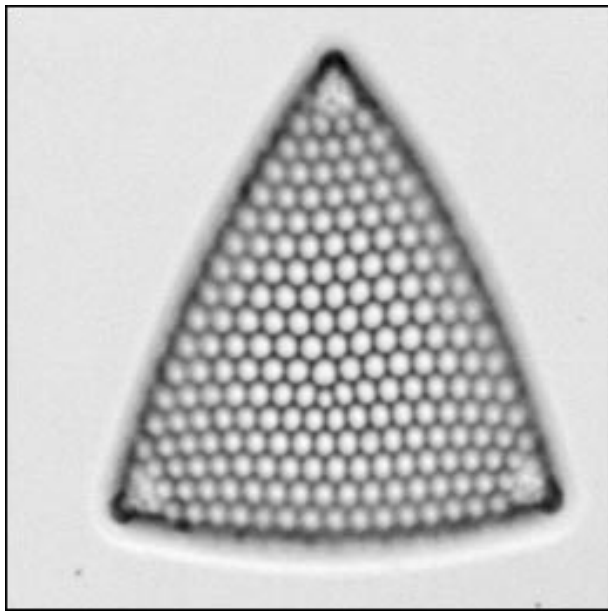
$$g_{i,j,k} = \int \int \int w(x, y, z) f(i+x, j+y, k+z) dx dy dz,$$

where $w(x, y, z)$ is the point spread function of the optical system and $f(x, y, z)$ denotes the optical density of the specimen at spatial location (x, y, z) . Many deconvolution methods, both linear and nonlinear, have been proposed for recovering f from g , using either a known or estimated w (see, for example, [5, 9, 11]).

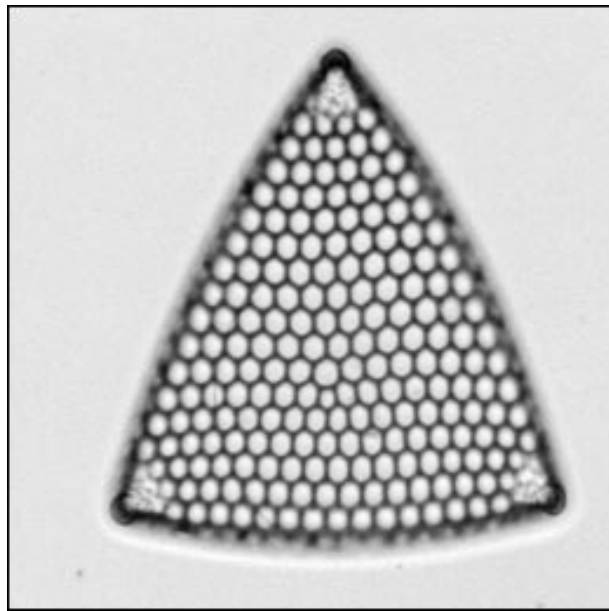
If a specimen can be considered to be two-dimensional, either because it is a thin section or because it is optically opaque so that only its top surface is imaged, then the extent of blur can be used to infer depth. It is assumed that

$$f(x, y, z) = \begin{cases} f'(x, y) & \text{if } z = z(x, y) \\ 0 & \text{otherwise,} \end{cases}$$

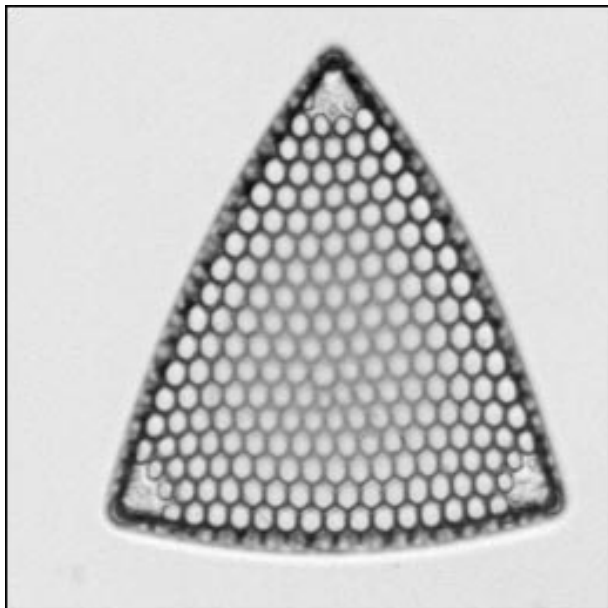
where $z(x, y)$ denotes the specimen position perpendicular to the focal plane and $f'(x, y)$ denotes the optical density. Darell and Wohn [2] and Nayar and Nakagawa [8] both determined $z(x, y)$, for each value of (x, y) , by the essentially ad hoc method of choosing the image plane (k) in which the output of a high-pass filter applied to g



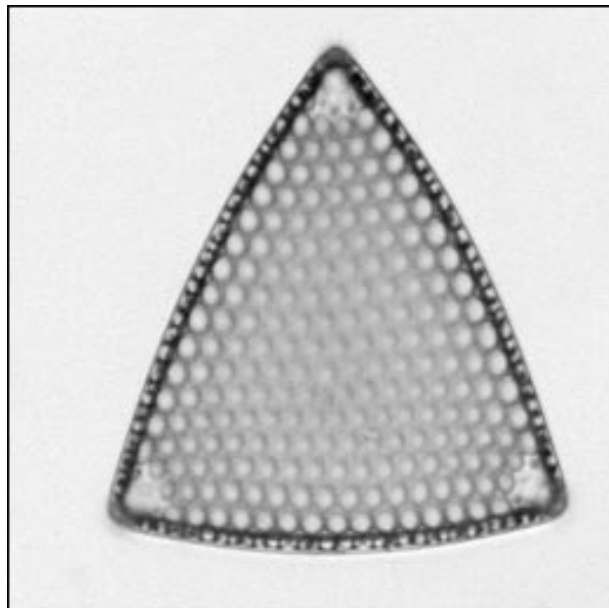
$k = 5$



$k = 7$



$k = 9$



$k = 11$

Figure 1: Diatom imaged in a brightfield microscope at 4 focal planes (k), a subset of a dataset of 14 focal planes, digitised to a 256×256 array with pixels in the range 0 to 255 [7].

was maximised. To illustrate, Fig 2 shows the estimated height of the top surface of the diatom, obtained from the series of fourteen optical sections (of which Fig 1 shows four) using this approach with Prewitt's gradient filter. The estimated height appears to be affected by noise, but is consistent with the centre of the diatom being higher than the edges.

Some form of smoothing could be used to produce visually more attractive results than Fig 2, but because the method is ad hoc, we cannot place confidence in the results. Deconvolution offers a more scientifically justifiable way to recover depth: by deconvolving g subject to the constraint that f is a two-dimensional surface, depth-from-focus and deconvolution are combined into a single algorithm. This is the subject of the paper. In section 2 we propose a computer-intensive method, and in section 3 we consider issues involved in parallel implementation.

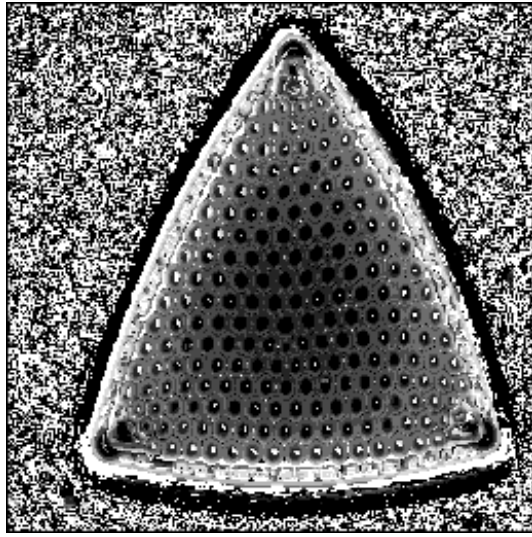


Figure 2: Representation of height of top surface of diatom, estimated using ad hoc depth-from-focus algorithm. Black areas denote where the surface lies in focal planes 1 to 5, white areas denote planes 11 to 14, and shades of grey denote intermediate planes.

Then, in section 4 we present results for the diatom images, before concluding, in section 5, with a discussion of generalisations.

2 Method

To estimate w , the point spread function, we assumed that the central part of the diatom was in focus in image plane 6. We constrained the elements in w to be non-negative, to decrease monotonically from $w(0,0,k)$ in each plane and to sum to unity within a 15×15 square. (We also considered constraining w to be isotropic in each plane, but found this to be incompatible with the data.) We then estimated w to minimise the sum of squares

$$\sum_{i=111}^{170} \sum_{j=111}^{170} \left(g_{i,j,6-l} - \sum_{x=-7}^7 \sum_{y=-7}^7 w(x,y,l) g_{i+x,j+y,6} \right)^2$$

separately for each value of l , using a quadratic programming algorithm to satisfy the linear constraints. Results at five focal planes are shown in Fig 3. We see that blur is not the same above as below the specimen surface.

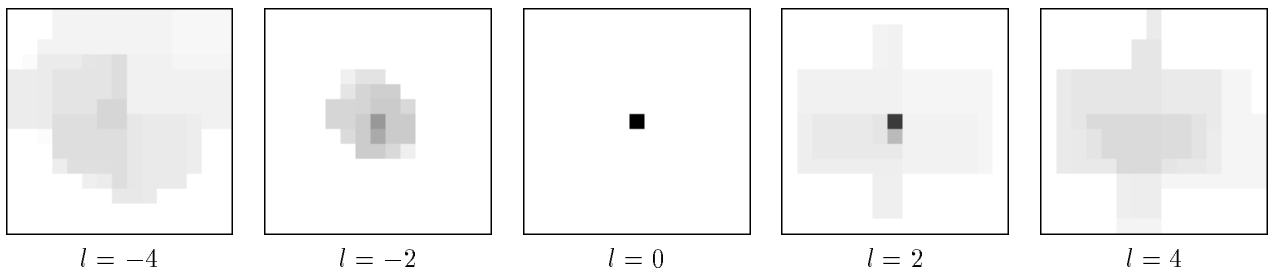


Figure 3: Estimated point spread function, $w(x,y,l)$, in a 15×15 square, with a coefficient equal to 1 displayed as black, 0 as white, and intermediate values as shades of grey.

The constrained deconvolution problem can be formulated to minimise a sum of squares plus roughness penalty

$$S = \sum_i \sum_j \sum_k e_{i,j,k}^2 + \beta \sum_x \sum_y \left\{ 2 - \frac{1}{1 + [z(x,y) - z(x-1,y)]^2/\delta^2} - \frac{1}{1 + [z(x,y) - z(x,y-1)]^2/\delta^2} \right\},$$

with respect to $z(x,y)$ and $f'(x,y)$. Here

$$e_{i,j,k} = g_{i,j,k} - \sum_x \sum_y w(x,y, z(x,y) - k) f'(i+x, j+y)$$

is the array of residuals, and β and δ are constants which define the roughness penalty. We found that if a roughness term were omitted then depths could not be estimated at all locations. This form of roughness penalty was proposed by Geman and McClure [3] and has since been widely used. It is locally-computable and does not excessively penalise step edges.

There is no analytic solution to minimise S . Therefore we must proceed iteratively. From initial values of f' and z , e and S are computed. Then, in a series of raster scans, each value of (x,y) within the outline of the diatom is considered in turn and f' is re-estimated. This is done by first setting $f'(x,y)$ to 0, by making changes

$$e_{x-i,y-j,k} \rightarrow e_{x-i,y-j,k} + w(i,j, z(i,j) - k) f'(x,y)$$

for all values of (i,j,k) , though only values for which $w(i,j, z(i,j) - k)$ is non-zero will be affected. Then we find a new value for $f'(x,y)$, to minimise S subject to the constraint $0 \leq f'(x,y) \leq 255$ (which makes physical sense and further helps to regularise the reconstruction). The solution is

$$f'(x,y) \rightarrow \begin{cases} 0 & \text{if } r < 0, \\ r & \text{if } 0 \leq r \leq 255, \\ 255 & \text{otherwise,} \end{cases}$$

where r is the unconstrained solution, namely

$$r = \frac{\sum_i \sum_j \sum_k e_{x-i,y-j,k} w(i,j, z(i,j) - k)}{\sum_i \sum_j \sum_k w(i,j, z(i,j) - k)^2}.$$

We repeat the calculations to estimate $f'(x,y)$ if the depth is simultaneously changed to

$$z(i,j) \rightarrow z(i,j) \pm \Delta,$$

for some small step increment Δ . Finally, we use simulated annealing [1] to choose between increasing or decreasing $z(i,j)$, or leaving it fixed. (This stochastic optimisation method was used to avoid becoming trapped in local minima of S .) Denote by S_1 , S_2 and S_3 the changed values of the criterion in these three cases, which are all locally computable. In the simulated annealing schedule, we choose option O with probability

$$\frac{e^{-S_O/T}}{e^{-S_1/T} + e^{-S_2/T} + e^{-S_3/T}},$$

where T is the ‘temperature’ of the process at this iteration. Then e and S are updated, and the next term (x,y) is considered in a raster fashion until, when every term has been considered, we have completed an iteration. Then we start the raster scan again. As iterations proceed, we slowly decrease T , until eventually we are following a gradient descent procedure. The algorithm terminates when, in a full raster scan, no changes are made to z , and S decreases by an arbitrarily small amount through refinements to f' .

3 Parallel implementation

The proposed method is computationally very intensive. Therefore we explored opportunities for parallelising the algorithm on a Cray-T3D at the Edinburgh Parallel Computing Centre. The halo size (that is, the number of neighbouring points needed to process a particular point) leads to problems in parallelisation. It is ± 7 in each direction, which is large in relation to the 256×256 grid size. Also, in processing a point we not only need to know the values of the neighbouring points in the halo, but also, after processing the point, we then need to update the

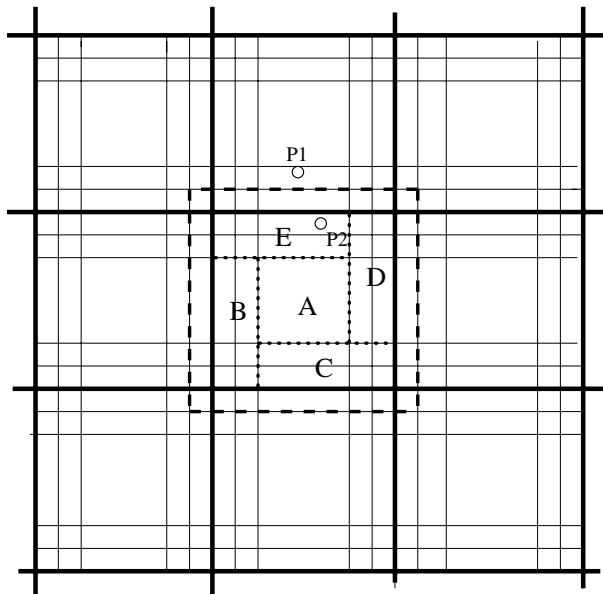


Figure 4: Ordering of points to keep communication to a minimum (see text).

surrounding halo. Therefore, the minimum data block size is 28×28 . High Performance Fortran (HPF), which is usually the simplest way to parallelise an algorithm, was unsuited to this problem because it does not allow parallelisation of loops where it detects data dependence conflicts. In other words, if the results of a calculation are not independent of whether the loop is carried out in serial or parallel, then HPF will not parallelise the loop. We therefore used Message Passing (MPI) instead.

It is possible to choose the order for processing the points to minimise the communications necessary between processors. One such method is shown in Fig 4. The two points P1 and P2 cannot be processed at the same time since they both depend on, and update, the points between them. However, all points in the centre squares, such as the one labelled A, can be processed in parallel. We can then go on to process all points in blocks such as the one labelled B in parallel, and so on. After processing each of the halo blocks, B, C, D and E, it is necessary to send the modified halos out to the neighbouring processors. However, by sending these modified regions out in large blocks rather than simply every time we process a single point in a halo region, we keep communications to a minimum.

Another aspect of critical importance to this problem is load balancing. This is due to the fact that points outside the specimen in the image require no processing. It is desirable to have an equal number of specimen points assigned to each processor. However, the specimen can be of arbitrary shape and size and perimeters of blocks (and hence halo areas) must be kept to a minimum. Several load sharing techniques were tried, although there is scope for more work here. Two of the more successful schemes are shown in Fig 5.

4 Results

The scaling of the code when running on the Cray-T3D was found to be limited by the quality of the load-sharing used. This is shown in Fig 6. Particularly noticeable here is the poorer than expected improvement for 64 processing elements (PEs), due to the minimum data block size for the algorithm being 28×28 . Hence the maximum speed increase which can be obtained is 26 fold, since all other processors do no work. A case could be made for modifying the algorithm to allow smaller block sizes (and hence allow more PEs to cover the specimen) although this would introduce a greater communication overhead, so it unclear whether this would lead to a speed increase.

After some experimentation, roughness parameters were set to $\beta = 20\,000$ and $\delta = 20$. The algorithm was started with all depths set to focal plane 6 and a simulated annealing temperature of 1000. A depth increment of $\Delta = 1/9$ was used and the temperature was reduced by 0.5% after every complete iteration. Final estimates of z and f' are displayed in Fig 7. The estimated height confirms that the centre of the diatom is higher than the

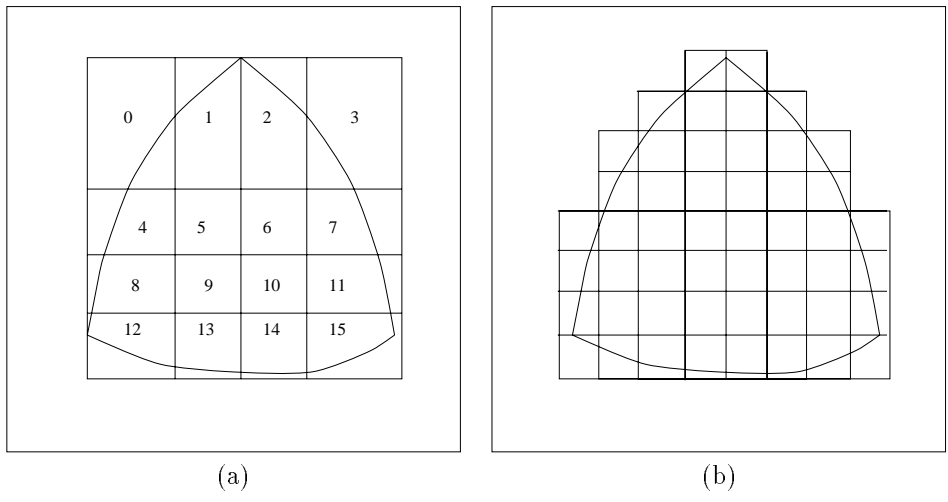


Figure 5: Two good load sharing schemes: (a) irregular sizes, (b) tiled.

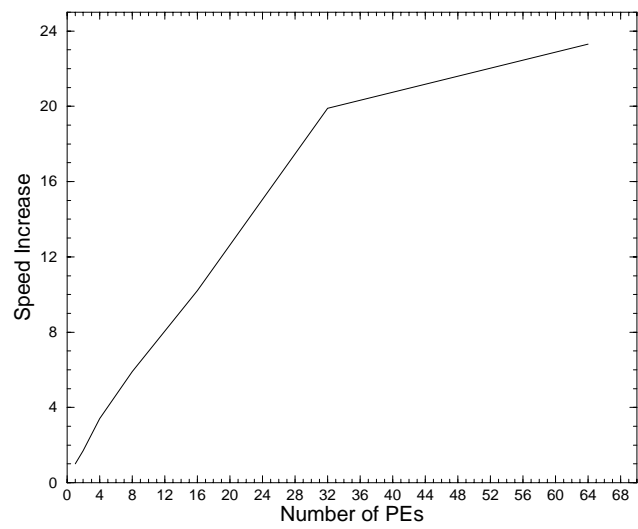


Figure 6: Graph showing speed-up of algorithm plotted against the number of processing elements (PEs).

edges, and is qualitatively similar to Fig 2. Fig 7(b) shows the digitally recovered image of the top surface of the diatom, everywhere in focus, which could not have been obtained by optical means.

5 Discussion

As we have shown, digital methods can facilitate the extraction of information from microscope images. The results in Fig 7 look promising. A simulation study is planned to further explore appropriate values for β , δ and the simulated annealing cooling schedule. Work is also underway to extend the method to recover more complicated specimen shapes where it cannot be assumed that a single surface is being imaged.

The development of specific algorithms in digital microscopy is difficult because the theory of optics is compli-

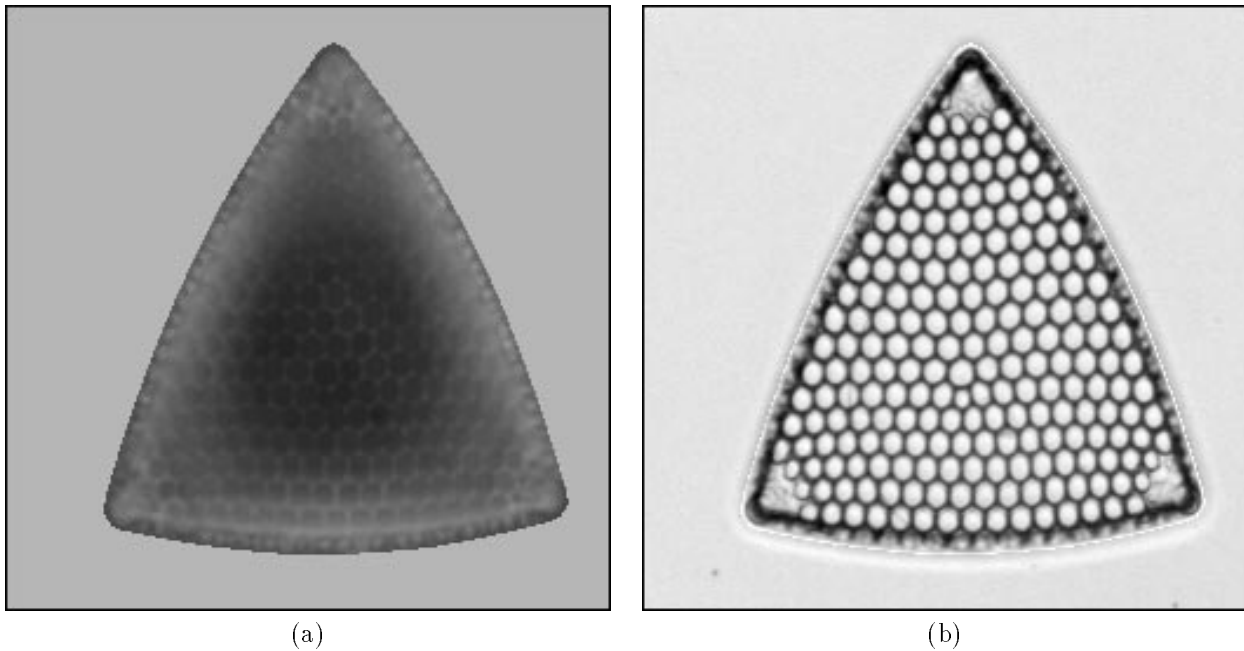


Figure 7: Estimated top surface of diatom, using deconvolution algorithm: (a) representation of the height of the surface, with black areas used to denote where the surface lies in focal planes 1 to 5, white areas denote planes 11 to 14, and shades of grey denote intermediate planes, (b) digitally recovered image of in-focus diatom.

cated, agreement with data is less than perfect [4] and there are many types of instrument, including brightfield, darkfield, phase contrast, interference contrast and fluorescence systems [10]. Generic image processing algorithms are often applied successfully, but they fail to exploit fully the information contained in microscope images. There is also a danger of misinterpretation if the optics which produced a particular image are not correctly understood. For example, the bas-relief type of images typical of differential interference contrast microscopy may be mistaken for three-dimensional features [12]. Much remains to be done to synthesise theoretical models and empirical evidence in order to tackle many of the problems which arise in optical microscopy.

Acknowledgements

We thank Ed Breen for permission to use the images in this paper. CAG's work was supported by funds from the Scottish Office Agriculture, Environment and Fisheries Department. MGP's work was supported by a Summer Scholarship at the Edinburgh Parallel Computing Centre, jointly supervised by Roger Hare, whose encouragement we gratefully acknowledge.

References

- [1] S.P. Brooks and B.J.T. Morgan, Optimization using simulated annealing, *The Statistician*, vol. 44, 1995, pp. 241-257.
- [2] T. Darell and K. Wohn, Depth from focus using a pyramid architecture, *Pattern Recognition Letters*, vol. 11, 1990, pp. 787-796.
- [3] S. Geman and D.E. McClure, Statistical methods for tomographic image construction, *Bulletin of the International Statistical Institute*, vol. LII-4, 1987, pp. 5-21.
- [4] C.A. Glasbey, D. Hitchcock, A.J.F. Russel and H. Redden, Towards the automatic measurement of cashmere-fibre diameter by image analysis, *Journal of the Textile Institute*, vol. 85, 1994, pp. 301-307.

- [5] C.A. Glasbey and G.W. Horgan, *Image Analysis for the Biological Sciences*, Wiley, Chichester, 1995.
- [6] S. Inoue, *Video microscopy*, Plenum Press, New York, 1986.
- [7] A. Lipton and E.J. Breen, On the use of local statistical properties in focusing microscopy images, *Microscopy Research and Techniques*, vol. 31, 1995, pp. 326-333.
- [8] S.K. Nayar and Y. Nakagawa, Shape from focus, *IEEE Transactions on Pattern Analysis and Machine Intelligence*, vol. 16, 1994, pp. 824-831.
- [9] C. Preza, M.I. Miller, J.T. Lewis and J.G. McNally, Regularized linear method for reconstruction of three-dimensional microscopic objects from optical sections, *Journal of the Optical Society of America, A*, vol. 9, 1992, pp. 219-228.
- [10] E.M. Slayter and H.S. Slayter, *Light and Electron Microscopy*, Cambridge University Press, Cambridge, 1992.
- [11] B. Willis, B. Roysam, J.N. Turner and T.J. Holmes, Iterative 3-D image reconstruction of transmitted light bright-field micrographs based on maximum likelihood estimation, *Journal of Microscopy*, vol. 169, 1993, pp. 347-361.
- [12] D. Young, C.A. Glasbey, A.J. Gray and N.J. Martin, Cell identification in differential interference contrast microscope images using template matching, In: *Proceedings of the 9th Scandinavian Conference on Image Analysis*, Uppsala, Sweden, June 1995, vol. 1, pp. 199-208.